



ELSEVIER

Contents lists available at ScienceDirect

Comptes Rendus Physique

www.sciencedirect.com



Propagation and remote sensing / Propagation et télédétection

New polarimetric signal subspace detectors for SAR processors

*Formation d'images SAR polarimétriques basée sur des détecteurs à sous-espace*Frédéric Brigui^{a,*}, Laetitia Thirion-Lefevre^a, Guillaume Ginolhac^b, Philippe Forster^b^a SONDRRA, Supélec, plateau de Moulon, 91190 Gif-sur-Yvette, France^b SATIE UniverSud, ENS Cachan, 94235 Cachan, France

ARTICLE INFO

Article history:

Available online 26 February 2010

Keywords:

SAR
Subspace detector
Polarimetric information

Mots-clés :

RSO
Détecteur à sous-espace
Information polarimétrique

ABSTRACT

Our studies aim at detecting targets embedded in a complex environment for radar applications. This article deals with new polarimetric SAR (synthetic aperture radar) processors based on subspace detectors. These algorithms use models of targets including physical and polarimetric properties of their scattering on the contrary to the isotropic point model that is commonly used. These processors are implemented by computing the corresponding subspaces that contain the relevant responses of the target. We choose for application the detection of targets under forest foliage. The obtained results both on simulated data of realistic targets and real data show the interest of these new processors.

© 2010 Académie des sciences. Published by Elsevier Masson SAS. All rights reserved.

R É S U M É

Nos études ont pour but la détection de cibles enfouies dans un environnement complexe pour des applications radar. Ce papier traite de nouveaux processeurs RSO (radar à synthèse d'ouverture) polarimétriques basés sur des détecteurs à sous-espace. Ces algorithmes utilisent des modèles de cibles incluant les propriétés physiques et polarimétriques de leur diffusion qui ne sont pas exploitées par le modèle de point isotrope généralement appliqué. Ces processeurs sont implementés en générant des sous-espaces qui contiennent les réponses d'intérêt de la cible. Nous présentons comme application la détection de cibles sous couvert forestier. Les résultats obtenus à la fois sur des données simulées de cibles réalistes et sur des données réelles montrent l'intérêt de ces nouveaux processeurs.

© 2010 Académie des sciences. Published by Elsevier Masson SAS. All rights reserved.

1. Introduction

The detection of Man Made Targets (MMT), embedded in random and structured noise, using a polarimetric SAR system is a current issue for both the signal processing and the SAR communities. Most of SAR detection algorithms consider targets as isotropic points and focus on noise properties [1,2]. However, the target scattering properties can be used to have a more suitable model. We previously developed new SAR processors based on subspace detectors to take into account the scattering properties of MMT in only one polarimetric channel [3,4]. In this paper, we consider all the polarization

* Corresponding author.

E-mail addresses: frederic.brigui@supelec.fr (F. Brigui), laetitia.thirion@supelec.fr (L. Thirion-Lefevre), guillaume.ginolhac@u-paris10.fr (G. Ginolhac), philippe.forster@u-paris10.fr (P. Forster).

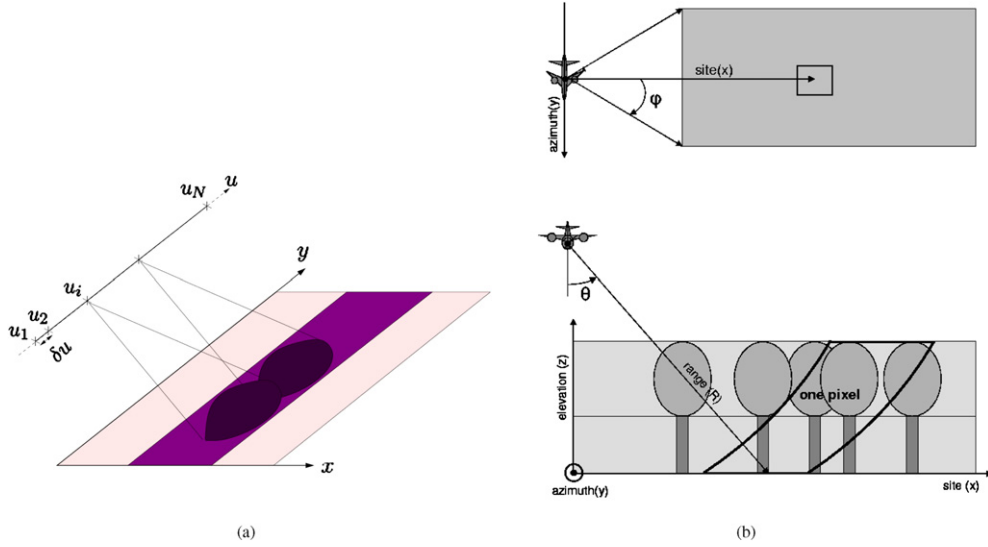


Fig. 1. (a) Geometric SAR configuration. An antenna evolves along a linear trajectory: $u_{i,i \in \llbracket 1, N \rrbracket}$ indicates its position and the distance δu between two successive locations is constant. The scene under observation is seen with different incident angles (see (b)) for several frequencies. (b) Incidence angles θ_i and φ_i of the emitted signal for a position u_i of the antenna.

Fig. 1. (a) Configuration géométrique du RSO. Une antenne évolue selon une trajectoire linéaire : $u_{i,i \in \llbracket 1, N \rrbracket}$ indique sa position et la distance δu entre deux positions successives est constante. La scène observée est vue sous différents angles d'incidence (voir (b)) pour plusieurs fréquences. (b) Angles d'incidence θ_i et φ_i du signal émis pour une position u_i de l'antenne.

channels in addition to the scattering properties of the target. For this purpose, we develop polarimetric SAR processors exploiting a target model based on its physical properties and namely its directional scattering pattern; the techniques used in [4] are extended to take into account polarimetric properties. We assume that the target scattering belongs to a low-rank polarimetric subspace. Considering all the configurations of a plate for all the polarization channels (HH and VV), we build processors based on an appropriate Generalized Likelihood Ratio (GLR) [5]. Since several possibilities are available to organize the polarimetric vectors, we develop new processors based on different preprocessing polarimetric decompositions; we show that these polarimetric preprocessing treatments are equivalent to classical post processing treatments in polarimetry [6]. Compared to a single polarization channel processor, these new polarimetric processors show important improvements in terms of probability of detection and robustness. This article is organized as follows. The detection problem is presented in Section 2. The use of a complex model with several degrees of freedom leads us to use a subspace detector. Section 3 describes the polarimetric target subspaces. Three cases depending on polarimetric decompositions are determined and related to their physical meaning. In Section 3.3, we discuss about the expressions of these new processors. Then in Section 4, we compare the performance of the polarimetric processors with those for a single polarization channel. Simulated data in white Gaussian noise and in structured noise are considered to test the ability and the robustness of these new processors. Finally we apply these processors to real FOPEN (Foliage Penetration) data. The following convention is adopted: italic indicates a scalar quantity, lower case boldface indicates a vector quantity and upper case boldface a matrix. T denotes the transpose operator and \dagger the transpose conjugate [7]. We adopt the BSA (Back Scattering Alignment) convention.

2. Polarimetric detection problem for an object with a directional scattering pattern

2.1. SAR configuration and notations

As shown in Fig. 1(a), the antenna evolves along a linear trajectory; at each position u_i , $i \in \llbracket 1, N \rrbracket$ the antenna emits a signal and receives the response from the scene under observation (see Fig. 1(b)). For more details on SAR configuration and process see [8]. The distance between adjacent positions is constant and equal to δu . The emitted signal is a chirp in polarization H or V with a frequency bandwidth B , a central frequency f_0 and a duration T_e . We denote by $\mathbf{z}_{pi} \in \mathbb{C}^K$ ($i \in \llbracket 1, N \rrbracket$) the received signal samples at every u_i position of the antenna either in horizontal polarization ($p = H$) or in vertical polarization ($p = V$) and K is the number of time samples; the total received signal \mathbf{z}_p for one polarization channel is the concatenation of the N vectors \mathbf{z}_{pi} (see [4]):

$$\mathbf{z}_p \in \mathbb{C}^{NK}, \quad \mathbf{z}_p = [\mathbf{z}_{p1}^T \quad \mathbf{z}_{p2}^T \quad \cdots \quad \mathbf{z}_{pN}^T]^T \quad (1)$$

The total polarimetric received signal \mathbf{z} is then the concatenation of \mathbf{z}_H and \mathbf{z}_V :

$$\mathbf{z} \in \mathbb{C}^{2NK}, \quad \mathbf{z} = [\mathbf{z}_H^T \quad \mathbf{z}_V^T]^T \quad (2)$$

2.2. Modeling and notations

To set the problem of detection, we define a model for the target. We suppose that a MMT can be seen as a canonical object or a set of identical canonical objects with different orientations. We suppose that the canonical object has an axis of symmetry, and thus its orientation in free space is totally defined by two angles (α, β) . To change the orientation of the object, we apply a first rotation of angle α about z -axis and then a second rotation of angle β about new y -axis. We consider that the target is initially oriented such as its axis of symmetry is parallel to the trajectory of the radar (for more details on these angles see [4]). For one SAR configuration and one received polarization channel p , we denote by $\mathbf{y}_p(\alpha, \beta)$ the vector containing the complex electromagnetic response of the canonical object to the emitted signal. We specify that $\mathbf{y}_p(\alpha, \beta)$ corresponds to the backscattering of an object located at the pixel (x, y) (or resolution cell (x, y)); for simplicity the dependence in (x, y) will not be written except if needed. Like the SAR received signal in Eq. (1), the vector $\mathbf{y}_p(\alpha, \beta)$ is described as follows:

$$\mathbf{y}_p(\alpha, \beta) \in \mathbb{C}^{NK}, \quad \mathbf{y}_p(\alpha, \beta) = [\mathbf{y}_{p1}^T(\alpha, \beta) \quad \mathbf{y}_{p2}^T(\alpha, \beta) \quad \dots \quad \mathbf{y}_{pN}^T(\alpha, \beta)]^T \quad (3)$$

where $\mathbf{y}_{pi}(\alpha, \beta)$ contains the electromagnetism response of the canonical model for an emitted signal of central frequency f_0 , for one position u_i of the antenna corresponding to incidence angles (θ_i, φ_i) and for one polarization channel p .

The total polarimetric model signal $\mathbf{y}(\alpha, \beta)$ is then:

$$\mathbf{y}(\alpha, \beta) \in \mathbb{C}^{2NK}, \quad \mathbf{y}(\alpha, \beta) = [\mathbf{y}_H^T(\alpha, \beta) \quad \mathbf{y}_V^T(\alpha, \beta)]^T \quad (4)$$

We define also the signal matrices \mathbf{Y}_p and \mathbf{Y} containing, respectively, all the vectors \mathbf{y}_p and \mathbf{y} for all the possible orientations (α_i, β_j) spanning $[0, \pi] \times [0, \pi]$:

$$\mathbf{Y}_p \in \mathbb{C}^{NK \times PQ}, \quad \mathbf{Y}_p = [\mathbf{y}_p(\alpha_1, \beta_1) \dots \mathbf{y}_p(\alpha_i, \beta_j) \dots \mathbf{y}_p(\alpha_P, \beta_Q)] \quad (5)$$

$$\mathbf{Y} \in \mathbb{C}^{2NK \times PQ}, \quad \mathbf{Y} = [\mathbf{y}(\alpha_1, \beta_1) \dots \mathbf{y}(\alpha_i, \beta_j) \dots \mathbf{y}(\alpha_P, \beta_Q)] \quad (6)$$

In practical terms we have to choose a sampling step for α_i and β_j to span $[0, \pi] \times [0, \pi]$; a criterion is presented in [4] to choose the biggest possible sampling step for the orientation angles. Indeed, we have to achieve a trade-off between an accurate description of all the possible values of \mathbf{y} and the computational cost it implies to derive the bases (see Section 3).

2.3. Detection problem

For each position (x, y) in the scene under observation, we can state the detection problem using the following binary hypotheses test. Either the received signal does not contain any target but only noise (H_0) or the received signal contains a target plus noise (H_1):

$$\begin{cases} H_0: \mathbf{z} = \mathbf{n} \\ H_1: \mathbf{z} = \mathbf{a}\mathbf{y}(\alpha, \beta) + \mathbf{n} \end{cases} \quad (7)$$

where $\mathbf{a} \in \mathbb{C}^{2NK}$ is a vector containing the complex attenuation coefficients for the different polarization channels, $\mathbf{n} \in \mathbb{C}^{2NK}$ is a complex Gaussian white noise vector of known variance σ^2 (for the unknown variance case, see [4]).

The orientation (α, β) of the target to detect is unknown, but we know the responses of this target for all its possible orientations:

$$\forall (\alpha, \beta) \in [\alpha_{\min}, \alpha_{\max}] \times [\beta_{\min}, \beta_{\max}], \mathbf{y}(\alpha, \beta) \in \langle H_{xy} \rangle \quad (8)$$

where $\langle H_{xy} \rangle$ is a polarimetric signal subspace of dimension D_H containing the vectors \mathbf{y} , the responses of the target for different orientations. We denote by \mathbf{H}_{xy} a $2KN \times D_H$ basis of this subspace. For one pixel (x, y) , the detection problem of Eq. (7) may then be rewritten as follows:

$$\begin{cases} H_0: \mathbf{z} = \mathbf{n} \\ H_1: \mathbf{z} = \mathbf{H}_{xy}\boldsymbol{\lambda} + \mathbf{n} \end{cases} \quad (9)$$

where $\boldsymbol{\lambda}_{xy} \in \mathbb{C}^{D_H \times 1}$ is an unknown coordinate vector.

As in [5,9], we propose to form the SAR image by choosing a monotonic function of the Generalized Likelihood Ratio Test (GLRT) [3,4] for the pixel value $I(x, y)$:

$$I(x, y) = \frac{\|\mathbf{H}_{xy}^\dagger \mathbf{z}\|^2}{\sigma^2} \quad (10)$$

The intensity $I(x, y)$ depends directly on the projection of \mathbf{z} into the signal subspace $\langle H_{xy} \rangle$; we will see in the next section how to form this subspace.

3. Bases computation

3.1. Polarimetric target model

Assuming that the scattering pattern of a MMT is directional, the isotropic point model used in classical SAR detectors is not suitable. A canonical element for the model may be more adapted to detect realistic targets. As in [3,4], the canonical element is chosen here to be a perfectly conducting (PC) plate whose backscattering is computed by means of physical optics approximation (PO). For a PC plate, the PO approximation gives rise to the nullity of the cross-polarized components (HV and VH) of the backscattered electric field; hence, only the HH and VV channels are considered in our study. Consequently, the subscripts H and V will refer to HH and VV. We have now to choose a way to arrange the HH and VV responses. Let $\mathbf{y}^{\text{co}+}(\alpha, \beta)$ be the concatenation of the signals backscattered by the target for the co-polarization channels:

$$\mathbf{y}^{\text{co}+}(\alpha, \beta) = \begin{pmatrix} \mathbf{y}_H(\alpha, \beta) \\ \mathbf{y}_V(\alpha, \beta) \end{pmatrix} \quad (11)$$

Moreover, in the PO approximation the PC property of the plate gives rise to the equality of the co-polarized electric backscattered fields: $\mathbf{y}_H(\alpha, \beta) = \mathbf{y}_V(\alpha, \beta) = \mathbf{y}_{PO}(\alpha, \beta)$ where $\mathbf{y}_{PO}(\alpha, \beta)$ is the vector containing the backscattering of the emitted signal by the PC plate for all the position u_i of the SAR and for one polarization channel in the PO approximation [7]. Therefore $\mathbf{y}^{\text{co}+}(\alpha, \beta)$ can be written as:

$$\mathbf{y}^{\text{co}+}(\alpha, \beta) = \begin{pmatrix} \mathbf{I}_{[NK \times NK]} & \mathbf{0}_{[NK \times NK]} \\ \mathbf{0}_{[NK \times NK]} & \mathbf{I}_{[NK \times NK]} \end{pmatrix} \mathbf{y}_{PO}(\alpha, \beta) \quad (12)$$

where $\mathbf{I}_{[NK \times NK]}$ is the identity matrix of dimensions $NK \times NK$. The co-polarization channels are in phase and have the same magnitude. Actually the scattering in Eq. (12) is similar to the backscattering by a sphere or a trihedral [7]. In [6], the trihedral backscattering is used to decompose any backscattered signals from random targets as well as the dihedral and the dipole contribution (the latter representing the HV contribution). Indeed, it is assumed that a polarimetric monostatic signal is well described by these three types of scattering (trihedral, dihedral and dipole scattering). This implies that the backscattering of a MMT is not totally described by $\mathbf{y}^{\text{co}+}(\alpha, \beta)$ and we may lose a part of the scattering information. To overcome this problem, we have to add the missing mechanisms. Knowing that the cross-polarized contributions are null, we introduce only the dihedral scattering with $\mathbf{y}^{\text{co}-}(\alpha, \beta)$:

$$\mathbf{y}^{\text{co}-}(\alpha, \beta) = \begin{pmatrix} \mathbf{I}_{[NK \times NK]} & \mathbf{0}_{[NK \times NK]} \\ \mathbf{0}_{[NK \times NK]} & -\mathbf{I}_{[NK \times NK]} \end{pmatrix} \mathbf{y}_{PO}(\alpha, \beta) \quad (13)$$

The co-polarization channels are opposite in phase and have the same magnitude which is similar to the backscattering of a dihedral in BSA convention [7]. We note that in the polarimetry community, the state of polarization in Eq. (12) is interpreted as single or odd-bounce scattering [6]. Eq. (13) describes the orthogonal state of polarization of the one in Eq. (12) and is interpreted as double or even-bounce scattering [6]. With these two models we fully describe the polarimetric backscattering of the PC plate. We will see in Section 4 with simulated and real data that the processors using $\mathbf{y}^{\text{co}+}(\alpha, \beta)$ or $\mathbf{y}^{\text{co}-}(\alpha, \beta)$ are able, in these particular cases, to distinguish polarimetric mechanisms.

3.2. Construction of the signal matrices

To implement the processors, we need to compute the bases of the signal subspaces. We firstly present the construction of the signal matrices which generates the different signal subspaces corresponding to the models $\mathbf{y}^{\text{co}+}(\alpha, \beta)$ and $\mathbf{y}^{\text{co}-}(\alpha, \beta)$. A third model called ‘decorrelated’ is developed too. It is shown in [10] that we can derive the bases of these subspaces using the Singular Value Decomposition (SVD) applied to the signal matrices. Finally we present the formulation of the intensities of the polarimetric SAR processors.

3.2.1. Definition of the signal matrix

Due to the equality of the co-polarization channels of the model in magnitude we have: $\mathbf{Y}_{Hxy} = \mathbf{Y}_{Vxy} = \mathbf{Y}_{xy}$. From the two models $\mathbf{y}^{\text{co}+}(\alpha, \beta)$ and $\mathbf{y}^{\text{co}-}(\alpha, \beta)$ we have two polarimetric signal matrices: $\mathbf{Y}^{\text{co}+}$ and $\mathbf{Y}^{\text{co}-}$; we define a third signal matrix \mathbf{Y}^{Deco} by considering the polarimetric information incoherently:

- (i) ‘‘Correlated +’’ case: we say that the HH and VV channels are positively correlated when the signal matrix is defined as follows

$$\mathbf{Y}_{xy}^{\text{Co}+} = \begin{pmatrix} \mathbf{Y}_{xy} \\ \mathbf{Y}_{xy} \end{pmatrix} \quad (14)$$

- (ii) ‘‘Correlated –’’ case: we say that the HH and VV channels are negatively correlated when the signal matrix is defined as follows

$$\mathbf{Y}_{xy}^{\text{Co-}} = \begin{pmatrix} \mathbf{Y}_{xy} \\ -\mathbf{Y}_{xy} \end{pmatrix} \quad (15)$$

(iii) “Decorrelated” case: the two polarization channels are independent

$$\mathbf{Y}_{xy}^{\text{Deco}} = \begin{pmatrix} \mathbf{Y}_{xy} & \mathbf{0}_{[NK \times PQ]} \\ \mathbf{0}_{[NK \times PQ]} & \mathbf{Y}_{xy} \end{pmatrix} \quad (16)$$

3.2.2. Construction of the signal bases

For one polarization channel, the basis \mathbf{H}_{xy}^p is obtained from the SVD of \mathbf{Y}_{xy} defined in Eq. (6):

$$\mathbf{Y}_{xy} = \mathbf{U}_{xy} \Sigma_{xy} \mathbf{V}_{xy}^\dagger \quad (17)$$

where \mathbf{U}_{xy} and \mathbf{V}_{xy} are the left and right singular vectors, and Σ_{xy} is a diagonal matrix containing the singular values. Then the basis \mathbf{H}_{xy}^p corresponds to the D_H first singular vectors of \mathbf{U}_{xy} associated to the D_H highest singular values. This quantity D_H is determined empirically: we have to achieve a trade-off between the detection of the target and the rejection of the noise. In practical terms, the SVD has a large computational cost; in [4], an original method has been developed to reduce the size of the signal matrix \mathbf{Y}_{xy}^p and to allow the computation of only one SVD for all the pixels (x, y) of the image.

Now, we will see how the bases $\mathbf{H}_{xy}^{\text{Deco}}$ and $\mathbf{H}_{xy}^{\text{Co}\pm}$ are obtained. For the “decorrelated” case, the matrices \mathbf{Y}_{Hxy} and \mathbf{Y}_{Vxy} are orthogonally arranged in $\mathbf{Y}_{xy}^{\text{Deco}}$ as shown in Eq. (16). We compute the SVD of $\mathbf{Y}_{xy}^{\text{Deco}}$:

$$\mathbf{Y}_{xy}^{\text{Deco}} = \mathbf{U}_{xy}^{\text{Deco}} \Sigma_{xy}^{\text{Deco}} \mathbf{V}_{xy}^{\text{Deco}\dagger} = \begin{pmatrix} \mathbf{U}_{xy} \Sigma_{xy} \mathbf{V}_{xy}^\dagger & \mathbf{0} \\ \mathbf{0} & \mathbf{U}_{xy} \Sigma_{xy} \mathbf{V}_{xy}^\dagger \end{pmatrix} \quad (18)$$

where $\mathbf{U}_{xy} \in \mathbb{C}^{NK \times PQ}$, $\mathbf{U}_{xy} = [\mathbf{u}_{1xy} \quad \mathbf{u}_{2xy} \quad \dots \quad \mathbf{u}_{PQxy}]$. Thereby, after arranging the singular values in Eq. (18) in descending order, $\mathbf{U}_{xy}^{\text{Deco}}$ has the form:

$$\mathbf{U}_{xy}^{\text{Deco}} = \begin{pmatrix} \mathbf{u}_{1xy} & \mathbf{0}_{[0, NK]} & \mathbf{u}_{2xy} & \dots & \mathbf{u}_{Mxy} & \mathbf{0}_{[0, NK]} \\ \mathbf{0}_{[0, NK]} & \mathbf{u}_{1xy} & \mathbf{0}_{[0, NK]} & \dots & \mathbf{0}_{[0, NK]} & \mathbf{u}_{Mxy} \end{pmatrix} \quad (19)$$

The basis $\mathbf{H}_{xy}^{\text{Deco}}$ consists in the $2D_H$ first columns of $\mathbf{U}_{xy}^{\text{Deco}}$. Due to the structure of $\mathbf{H}_{xy}^{\text{Deco}}$, the polarimetric information is treated separately in the polarimetric subspace $\langle H_{xy}^{\text{Deco}} \rangle$.

In the “correlated” cases in Eq. (14) and Eq. (15), the signal matrices $\mathbf{Y}_{xy}^{\text{Co}\pm}$ are expressed as $\mathbf{Y}_{xy}^{\text{Co}\pm} = \begin{pmatrix} \mathbf{Y}_{xy} \\ \pm \mathbf{Y}_{xy} \end{pmatrix}$. The SVDs of $\mathbf{Y}_{xy}^{\text{Co}\pm}$ can be written as:

$$\mathbf{Y}_{xy}^{\text{Co}\pm} = \mathbf{U}_{xy}^{\text{Co}\pm} \sqrt{2} \Sigma_{xy} \mathbf{V}_{xy}^\dagger \quad (20)$$

with

$$\mathbf{U}_{xy}^{\text{Co}\pm} = \begin{pmatrix} \frac{1}{\sqrt{2}} \mathbf{U}_{xy} \\ \pm \frac{1}{\sqrt{2}} \mathbf{U}_{xy} \end{pmatrix} \quad (21)$$

The basis $\mathbf{H}_{xy}^{\text{Co}\pm}$ consists then in the D_H first columns of $\mathbf{U}_{xy}^{\text{Co}\pm}$.

Contrary to $\mathbf{H}_{xy}^{\text{Deco}}$, each vector of $\mathbf{H}_{xy}^{\text{Co}\pm}$ describes the two polarization channels. Moreover the subspaces $\langle H_{xy}^{\text{Co}\pm} \rangle$ have a lower dimension than $\langle H_{xy}^{\text{Deco}} \rangle$. As written above, the bases $\mathbf{H}_{xy}^{\text{Deco}}$ and $\mathbf{H}_{xy}^{\text{Co}\pm}$ have to be computed for all pixels of the image which represents a huge computational cost. However, a method for using only one SVD for all pixels in [4] allows one to perform these computations in realistic SAR configurations.

3.3. Formulation of the intensities

As seen in Section 2, the pixel intensity at (x, y) depends on the projection of the received signal \mathbf{z} into the polarimetric signal subspace. For the “decorrelated” case, the intensity of a pixel is expressed as follows:

$$I^{\text{Deco}}(x, y) = \frac{\|\mathbf{H}_{xy}^{\text{Deco}\dagger} \mathbf{z}\|^2}{\sigma^2} = \frac{\|\mathbf{H}_{xy}^{H\dagger} \mathbf{z}_H\|^2}{\sigma^2} + \frac{\|\mathbf{H}_{xy}^{V\dagger} \mathbf{z}_V\|^2}{\sigma^2} = I_H(x, y) + I_V(x, y) \quad (22)$$

The SAR processor for the intensity I^{Deco} is named the SDSAR Deco (Subspace Detector SAR Decorrelated). As well, the processors giving the intensity I_H and I_V are named the SDSAR HH and the SDSAR VV and have been previously developed in [3,4]. The use of the “decorrelated” detector leads to apply the processor to the HH and VV channels separately. In this case, the phase information between the two channels is lost.

For the “correlated” cases, the intensities are:

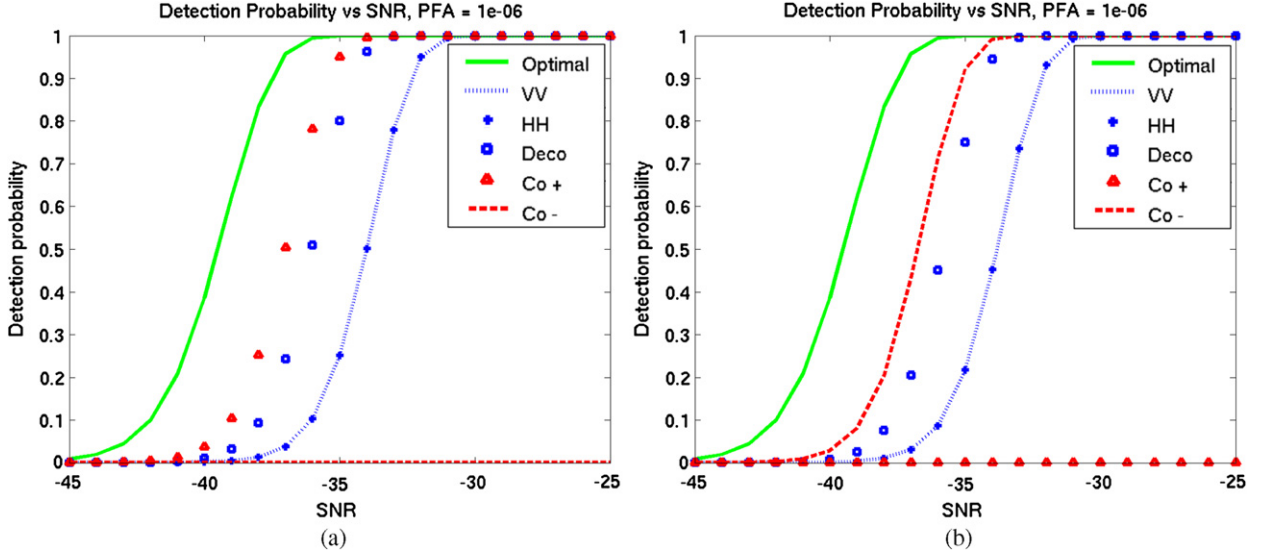


Fig. 2. Detection probability versus SNR for (a) a PC flat plate in white Gaussian noise of (2 m × 1 m) and (b) a PC box of size (2 m × 1.5 m × 1 m) over a PC flat ground, for an emitted signal of central frequency of 400 MHz with a bandwidth of 100 MHz.

Fig. 2. Probabilité de détection en fonction du RSB (rapport signal à bruit) pour (a) une PC plaque plate de dimensions (2 m × 1 m) et une boîte PC de dimensions (2 m × 1,5 m × 1 m) sur un sol plat PC, pour un signal émis de fréquence centrale 400 MHz avec une bande de fréquence de 100 MHz.

$$I^{\text{Co}+}(x, y) = \frac{\|\mathbf{H}_{xy}^{\text{Co}+\dagger} \mathbf{z}\|^2}{\sigma^2} = \frac{1}{2} \frac{\|\mathbf{H}_{xy}^{\dagger} \mathbf{z}_H + \mathbf{H}_{xy}^{\dagger} \mathbf{z}_V\|^2}{\sigma^2} \quad (23)$$

$$I^{\text{Co}-}(x, y) = \frac{\|\mathbf{H}_{xy}^{\text{Co}-\dagger} \mathbf{z}\|^2}{\sigma^2} = \frac{1}{2} \frac{\|\mathbf{H}_{xy}^{\dagger} \mathbf{z}_H - \mathbf{H}_{xy}^{\dagger} \mathbf{z}_V\|^2}{\sigma^2} \quad (24)$$

The processors described by Eq. (23) and Eq. (24) are respectively named the SDSAR Co+ and the SDSAR Co-. We clearly see that the intensities of the “correlated” processors are the sum or the difference of the projections of \mathbf{z}_H and \mathbf{z}_V into the basis \mathbf{H}_{xy} . In polarimetry, the sum of the HH and VV channels corresponds to a single bounce scattering and the difference, to double bounce scattering; in fact we retrieve the Pauli decomposition [6] used in radar image post processing. Thus, targets with different polarimetric properties will be treated differently with the two “correlated” processors.

4. Application

In this section, the new polarimetric processors, SDSAR Deco, SDSAR Co- and SDSAR Co+ are applied to simulated and real data; we compare their performance to that of the SDSAR VV in white noise, in structured noise (forest) and in real noise (real SAR data). In Sections 4.1 and 4.2, the signal subspaces are generated with (2 m × 1 m) PC plates. The sampling step for orientation angles is 9° and the rank D_H defined in Eq. (21) is 10 except for the decorrelated subspace which has a rank of 20.

4.1. Simulation in white noise

We are interested in evaluating and comparing the performance of the polarimetric detectors in white Gaussian noise. We focus in this study on the probability of detection but other quantities such as the probability of false alarm and of non-detection can also be computed. The SAR processors are first tested on simulated data. We consider a flight between the first position $u_1 = -50$ m and the last position $u_{200} = 50$ m with $\delta_u = 0.5$ m between each position and an altitude of 100 m. The polarimetric emitted signal is a chirp with a central frequency of 400 MHz with a bandwidth of 100 MHz and with a duration of 2×10^{-7} s. Finally, the radar scene is a (50 m × 45 m) rectangle. Two targets with different polarimetric signatures are placed at the center of the scene under observation: a (2 m × 1 m) PC plate in free space (there is no ground in this case) whose scattering is computed using PO approximation [7,4], and a PC box with a size of (2 m × 1.5 m × 1 m) over a PC flat ground whose scattering is simulated using Feko [11]. Both targets are oriented such as their broader dimension is parallel to the airborne flight. The targets are embedded in a white Gaussian noise. We represent in Figs. 2(a) and 2(b) the probability of detection for the new detectors Co+, Co-, Deco and for the detectors using a single polarization channel (HH and VV). In this case we observe that we obtain the same results for the two polarization channels due to the fact that HH = VV for the backscattering of a PC plate simulated using the PO approximation. We represent also the optimal case corresponding to a match filtering of the received signal by the response of the target. In Fig. 2(a), we notice that the SDSAR Deco, which does not exploit the polarimetric information, allows already a 2 dB gain in comparison with the SDSAR

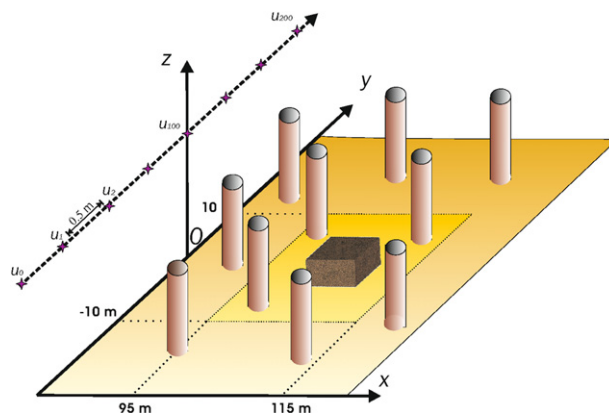


Fig. 3. Scene configuration for the simulated data. A PC box of size $(2 \text{ m} \times 1.5 \text{ m} \times 1 \text{ m})$ over a PC flat ground is placed in a forest of dielectric trunks, for an emitted signal of central frequency of 400 MHz with a bandwidth of 100 MHz.

Fig. 3. Configuration de la scène pour les données simulées. Une boîte PC de dimension $(2 \text{ m} \times 1,5 \text{ m} \times 1 \text{ m})$ sur un sol plat PC est placée dans une forêt de troncs diélectriques, pour un signal émis de fréquence centrale 400 MHz avec une bande de fréquence de 100 MHz.

VV (or SDSAR HH). The best performance is obtained using the SDSAR Co+, as we have now a 3 dB gain compared to the SDSAR VV. However, the SDSAR Co− does not detect the plate. This means that we have detected the mechanism scattering associated to $(\text{HH} + \text{VV})$. In BSA, this corresponds to the trihedral scattering (or single scattering). This matches perfectly the scattering by a plate in free space. In Fig. 2(b), we have the same results except that we have to use the SDSAR Co− to detect the box lying over a flat ground. This means that we have detected the scattering mechanism associated to $(\text{HH} - \text{VV})$. In BSA, this corresponds to the dihedral scattering (double scattering) and actually, the interactions between the ground and the box are now dominant. This matches the dominant scattering by a box on a flat ground.

These results show firstly the increase of the performance in white noise allowed by the use of the polarimetric information and secondly the robustness of the processors since we can detect a box over a ground with a subspace generated using the scattering of plates in free space. Finally, the SDSAR Co+ and the SDSAR Co− allow us to identify scattering mechanisms and so to distinguish different types of targets.

4.2. Simulation in a forest

Previously, we showed the performance of the processors in white Gaussian noise. Here we are interested in the performance of the processors in structured clutter and the ability of the processors to discriminate between a target and an interference (which is a structured clutter). Hence, we consider the same SAR configuration as previously but the scene is different. The target is a PC box lying over a PC flat ground located approximately at the center of the scene. Furthermore the target is placed into a simulated forest (see Fig. 3). At the frequencies used in our simulations ($f_0 = 400 \text{ MHz}$, $B = 100 \text{ MHz}$), the principal cause of the false alarms are the interferences due to the scattering of the trunks of the trees. Thus, only the scattering of the trunks are simulated with COSMO [12,13], a software dedicated to the study of radar scattering by forests. The target is placed in a forest of dielectric trunks with a height of 11 m and a radius of 20 cm. We represent in Fig. 4, the image provided by the SDSAR VV; as in [4], the response of the box is higher to that of the trunks. The detector SDSAR VV is adapted to the detection of MMT and thus the trunks have a low response. Furthermore, for the frequencies used and for the VV polarization channel, the trunks have generally a low response which is not the case at HH polarization. In Fig. 5, we represent the images obtained for the same scene using the SDSAR Co− and the SDSAR Co+. First, we see that in Fig. 5(a) the target is detected which is not the case in Fig. 5(b). We retrieve of course the same result than in Fig. 2(b): the box over a ground is detected by the SDSAR Co− and not by the SDSAR Co+ as the main scattering mechanism is the interactions between the box and the ground. Secondly, compared to the SDSAR VV, the SDSAR Co− slightly increases the response of the trunks compared to the box. As with the SDSAR Co−, we detect the double-bounce scattering mechanism, we increase also the responses of the trunks (because of their interactions with the ground). Moreover, in our case, the ground–trunk interactions are larger than the ground–box ones. Consequently, the use of polarimetric information slightly increases the false alarms due to the trunks. Actually, the SDSAR VV still has a better performance to discriminate target from trunks at the frequencies used. Nevertheless, we can now distinguish the different scattering mechanisms which is a first step for target identification.

4.3. Real data

To validate the previous results on simulated data, we apply the processors SDSAR VV, Co+ and Co− to real data. The real SAR data presented in this section have been acquired during the PYLA 2004 campaign (Landes, France), using the SAR system RAMSES from ONERA (the French Aerospace Lab) at frequencies between 400 MHz and 470 MHz and with

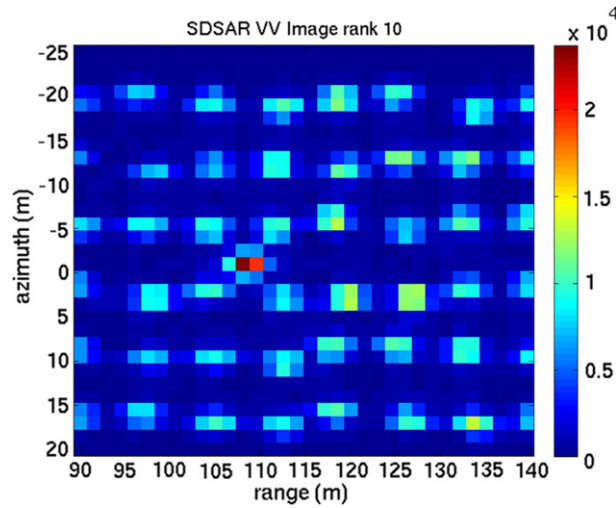


Fig. 4. SDSAR VV image (absolute value of the intensity) with $D_H = 10$ of a PC box over a PC ground in a simulated forest of trunks. The box appears clearly throughout the forest of trunks.

Fig. 4. Image SDSAR VV (l'échelle des intensités est linéaire) avec $D_H = 10$ d'une boîte PC sur sol plat et PC dans une forêt simulée de troncs. La boîte apparaît clairement à travers la forêt de troncs.

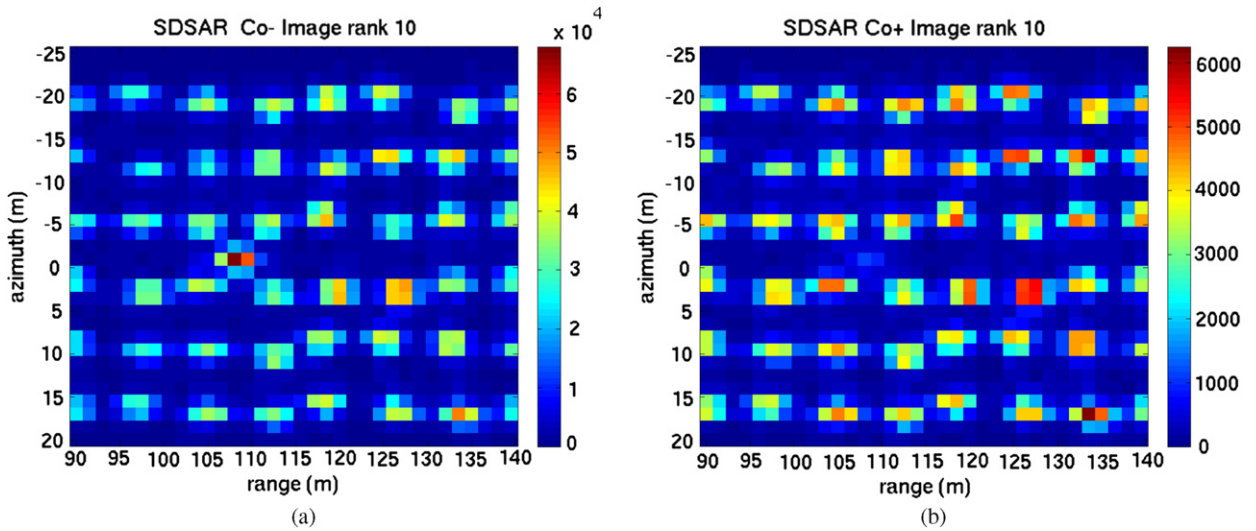


Fig. 5. (a) SDSAR Co– image (absolute value of the intensity) with $D_H = 10$ of a PC box over a PC flat ground in a simulated forest of trunks. The box has almost the same intensity than the trunks and is not really distinct from the interferences as in Fig. 4. (b) SDSAR Co+ (absolute value of the intensity) image with $D_H = 10$ of a PC box over a PC ground in a simulated forest of trunks. The box is no more detected.

Fig. 5. (a) Image SDSAR Co– (l'échelle des intensités est linéaire) avec $D_H = 10$ d'une boîte PC sur sol plat et PC dans une forêt simulée de troncs. La boîte a presque la même intensité que les troncs et n'est pas facilement différenciable des interférences comme dans la Fig. 4. (b) Image SDSAR Co+ (l'échelle des intensités est linéaire) avec $D_H = 10$ d'une boîte PC sur sol plat et PC dans une forêt simulée de troncs. La boîte n'est plus détectée.

an incidence angle of 59.8° . For more details on the Nezer forest, see [13]. Two targets, a truck and a trihedral corner reflector, with an orientation parallel to the radar flight have been placed in the forest and are represented in Fig. 6. We use $2\text{ m} \times 1\text{ m}$ PC plates to generate the signal subspaces. The sampling step for the orientation angles is 9° and the rank D_H of the subspaces is 10.

For comparison, we first represent the image using the SDSAR VV in Fig. 7. Both the two targets are easily detected and especially in comparison to the classical processor SAR [4].

In Figs. 8(a) and 8(b), we represent the images of the SDSAR Co– and SDSAR Co+. First, the performance of detection of the targets is increased in the two images; we retrieve the gain of detection in Figs. 2(a) and 2(b) obtained with simulated data in white noise. Secondly, the false alarms due to the trunks are quite the same between the SDSAR VV in Fig. 7 and the polarimetric SDSAR Co+ and Co– respectively in Figs. 8(a) and 8(b). Finally, the truck is detected by the SDSAR Co– whereas the trihedral is detected by the SDSAR Co+. Indeed, the dominant response of the truck is due to the interactions between

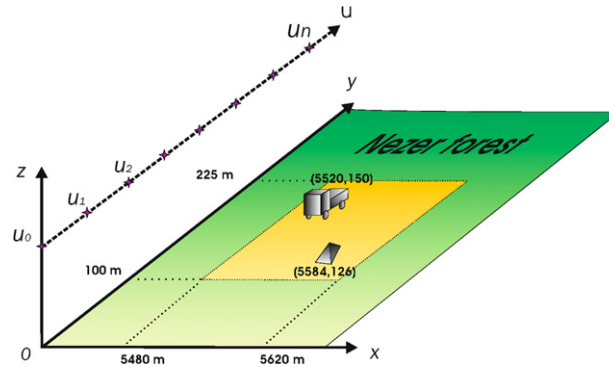


Fig. 6. Radar scene of the real data. A truck and a trihedral are placed in the forest of Nezer. The scene is observed at different frequencies between 400 MHz and 470 MHz and with an incidence angle of 59.8° .

Fig. 6. Scène radar des données réelles. Un camion et un trièdre sont placés dans la forêt de Nezer. La scène est observée à différentes fréquences entre 400 MHz and 470 MHz et avec un angle d'incidence de 59.8° .

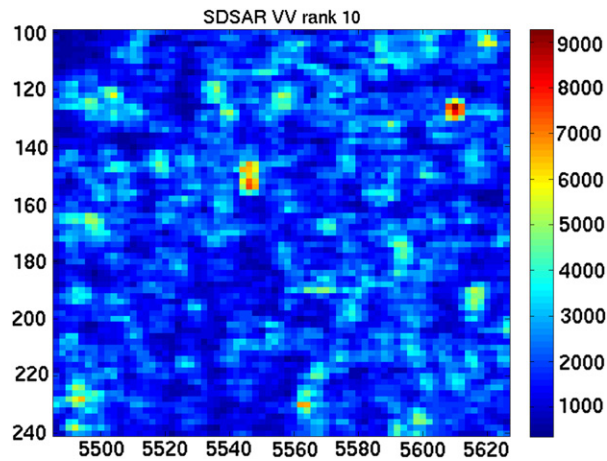


Fig. 7. SDSAR VV image (absolute value of the intensity) with $D_H = 10$ of a truck and a trihedral corner reflector in the Nezer forest (PYLA 2004 SAR data). The two targets are well detected throughout the forest.

Fig. 7. Image SDSAR VV (l'échelle des intensités est linéaire) $D_H = 10$ d'un camion et d'un trièdre dans la forêt de Nezer (données SAR de PYLA 2004). Les deux cibles sont bien détectées à travers la forêt.

the truck and the ground. We thus identify the scattering mechanism of a dihedral. As well, we identify the scattering mechanism of a trihedral with the SDSAR Co+. This means that our SAR processors besides detecting targets are able to identify them through their polarimetric properties. These results on real data confirm the performance of detection of the SDSAR Co- and Co+. Furthermore, we have successfully tested the robustness of these new processors to real configuration. Finally, the use of polarimetric information allows us to perform detection and identification at the same time.

5. Conclusion

We presented in this article new polarimetric SAR processors based on subspace detectors and polarimetric decomposition. By using other models than isotropic point and by taking in consideration the target polarimetric information, we have developed new processors whose models correspond to different scattering mechanisms: the dihedral and the trihedral scattering. The performance of simulated data in white noise of the polarimetric processors outperforms the processors using one polarization channel. Even if the discrimination between the target and the interferences in terms of intensity can be decreased with the processors Co+ and Co-, the false alarm level still remains acceptable. Furthermore, results on real data show the robustness of our processors to detect real MMTs in a real environment. Finally, the processors Co+ and Co- have a new ability of identifying the scattering mechanisms without additional treatment.

For future work, many ways have to be explored. First, we can investigate further the evaluation of the performance of our processors. The probability of false alarm will quantify the ability of our processors to distinguish target between white Gaussian noise and structured clutter; the probability of non-detection will quantify the robustness of our models. Then, the physical signification of the new images Co+ and Co- has to be studied since we use complex models compared to the isotropic point classically used. Other treatments to reduce false alarms could be implemented to improve the performance

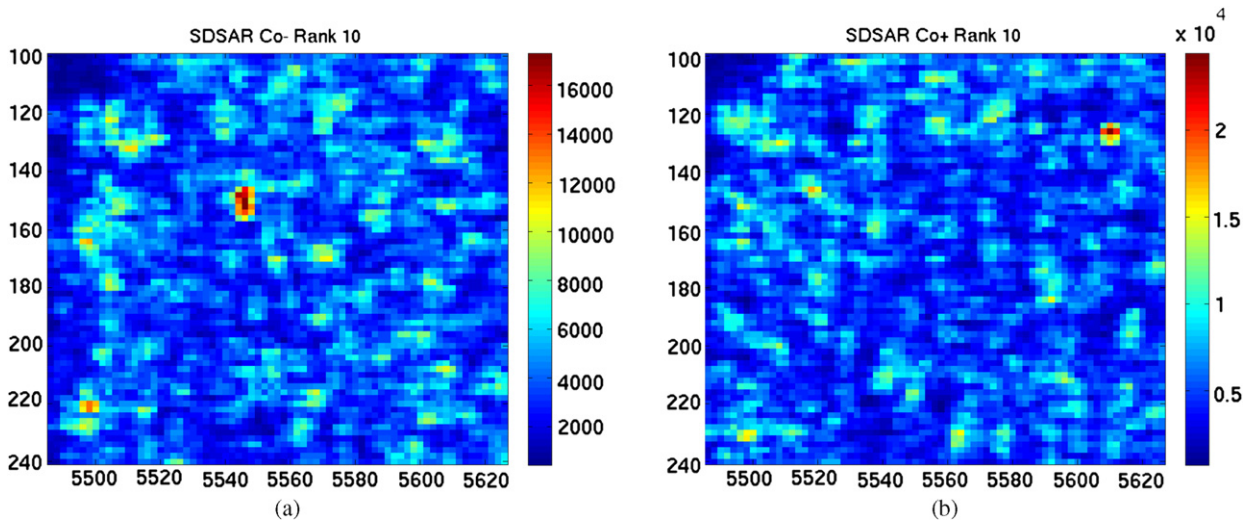


Fig. 8. (a) Image SDSAR Co– image (absolute value of the intensity) with $D_H = 10$ of a truck and a trihedral corner reflector in the Nezer forest (PYLA 2004 radar data). Only the truck is detected. (b) SDSAR Co+ image (absolute value of the intensity) with $D_H = 10$ of a truck and a trihedral corner reflector in the Nezer forest (PYLA 2004 radar data). Only the trihedral corner reflector is detected.

Fig. 8. (a) Image SDSAR Co– (l'échelle des intensités est linéaire) $D_H = 10$ d'un camion et d'un trièdre dans la forêt de Nezer (données SAR de PYLA 2004). Seul le camion est détecté. (b) Image SDSAR Co+ (l'échelle des intensités est linéaire) $D_H = 10$ d'un camion et d'un trièdre dans la forêt de Nezer (données SAR de PYLA 2004). Seul le trièdre est détecté.

of the processors as in [3]. Finally, we have to extend our processors to the cross-polarization channels and also to develop more optimal polarimetric decompositions for specific applications.

Acknowledgements

The authors would like to address their thank to the Direction Générale de l'Armement (DGA) for funding this project. We also thank the ONERA for providing us the PYLA 2004 data.

References

- [1] L.M. Novak, M.B. Sechtin, M.J. Cardullo, Studies of target detection algorithms that use polarimetric radar data, *IEEE Trans. Aerosp. Electron. Syst.* 25 (2) (March 1989) 150–165.
- [2] D. Pastina, P. Lombardo, T. Bucciarelli, Adaptive polarimetric target detection with coherent radar, part I, *IEEE Trans. Aerosp. Electron. Syst.* 37 (4) (October 2001) 1194–1206.
- [3] R. Durand, G. Ginolhac, P. Forster, L. Thirion-Lefèvre, SAR processor based on signal or interference subspace detector matched to man made target in a forest, in: ICASSP, Hawaii, USA, April 2007.
- [4] R. Durand, G. Ginolhac, L. Thirion-Lefèvre, P. Forster, New SAR processor based on matched subspace detector, *IEEE Trans. Aerosp. Electron. Syst.* 45 (1) (January 2009) 221–236.
- [5] L.L. Scharf, *Statistical Signal Processing: Detection, Estimation and Time Series Analysis*, Addison-Wesley Publishing Co., 1990.
- [6] L. Ferro-Famil, C. Lopez-Martinez, E. Pottier, *Polsarpro Manual, Part I, Chapter 4*, <http://earth.esa.int/polsarpro/Manuals/4PolarimetricDecompositions.pdf>.
- [7] F.T. Ulaby, C. Elachi (Eds.), *Radar Polarimetry for Geoscience Application*, Artech House Publishers, Norwood, MA, 1990.
- [8] M. Soumekh, *Synthetic Aperture Radar Signal Processing with Matlab Algorithms*, Wiley-Interscience, 1999.
- [9] L.L. Scharf, B. Friedlander, Matched subspace detectors, *IEEE Trans. Signal Process.* 42 (8) (August 1994) 2146–2157.
- [10] P. Forster, Generalized rectification of cross spectral matrices for array of arbitrary geometry, *IEEE Trans. Signal Process.* 49 (5) (2001) 972–978.
- [11] Feko, *User's Manual*, EM Software and System, 2004.
- [12] L. Thirion, I. Chênerie, C. Galy, Application of a coherent model in simulating the backscattering coefficient of mangrove forest, *Waves Random Media* 14 (2) (April 2004) 299–316.
- [13] L. Thirion, E. Colin, C. Dahon, Capabilities of a forest coherent scattering model applied to radiometry, interferometry and polarimetry at P- and L-bands, *IEEE Trans. Geosci. Remote Sens.* 44 (4) (April 2006) 849–862.